Inorganic Chemistry

Article

pubs.acs.org/IC

Synergy in Photomagnetic/Ferromagnetic *Sub*-50 nm Core-Multishell Nanoparticles

Nada Dia,[†,∥] Laurent Lisnard,*[,†,‡] Yoann Prado,[†] Alexandre Gloter,[§] Odile Stéphan,[§] François Brisset,[†] Hala Hafez,[∥] Zeinab Saad,[∥] Corine Mathonière,*[,⊥,⊗] Laure Catala,*[,†] and Talal Mallah[†]

[†]Institut de Chimie Moléculaire et des Matériaux d'Orsay, rue du Doyen Poitou, Université Paris Sud 11, 91405 Orsay, France

[‡]Institut Parisien de Chimie Moléculaire, UMR CNRS 7201, UPMC Université Paris 06, 4 Place Jussieu, 75005 Paris, France

[§]Laboratoire de Physique des Solides, UMR 8502, Université Paris-Sud 11, F-91405 Orsay, France

[∥]Ecole Doctorale des Sciences et de Technologie, Université Libanaise, Hadath campus P.O. Box 5, Beyrouth, Liban

[⊥]CNRS, ICMCB, UPR 9048, F-33600 Pessac, France

[⊗]University of Bordeaux, ICMCB, UPR 9048, F-33600 Pessac, France

Supporting Information

ABSTRACT: Based on nickel hexacyanidochromate and cobalt hexacyanidoferrate Prussian blue analogues, two series of photomagnetic/ferromagnetic *sub*-50 nm core multishell coordination nanoparticles have been synthesized in a surfactant-free one-pot multistep procedure with good control over the dispersity (10% standard deviation) and good agreement with the targeted size at each step. The composition and the valence state of each shell have been probed by different techniques that have revealed the predominance of Co^{II}-NC-Fe^{III} pairs in a series synthesized without alkali while Co^{III}-NC-Fe^{II} photoswitchable pairs have been successfully obtained in the photoactive coordination nanoparticles by control of Cs^+ insertion. When compared, the photoinduced behavior of the latter compound is in good agreement with that of the model one. Exchange coupling favors a uniform reversal of the magnetization of the heterostructured nanoparticles, with a large magnetization brought by a soft ferromagnetic shell and a large coercivity due to a harder photomagnetic shell. Moreover, a persistent *increase* of the photoinduced magnetization is observed for the first time up to the ordering temperature (60 K) of the ferromagnetic component because of a unique synergy.

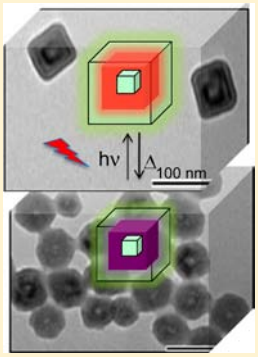

INTRODUCTION

Magnetic nanoparticles made of coordination networks are at the forefront of research on multifunctional molecular materials. Indeed, coordination chemistry offers a rich modulation of the network architecture and electronic properties, and when confined to the nanoscale, original coordination-network-based nanoparticles (CNPs) useful for information storage or sensing applications may be designed. As for the bulk compounds,[1−6] their physical behavior (magnetic, optical, etc.) can also be tuned and monitored by an external stimulus such as a magnetic or electric field,[7] light,[8] pressure or temperature,[9] leading to switchable bistable nano-objects.

Bimetallic cyanide-based coordination networks such as Prussian blue analogues (PBAs) give a nice illustration of the tunable properties obtainable by simply changing the nature of the metal ions within the scaffold. Among them, ferromagnets such as $Cs[Ni^{II}Cr^{III}(CN)_6]$ (notated as CsNiCr), with high Curie temperatures (T_c = 90 K)[10] and photomagnets such as cobalt hexacyanidoferrate PBAs (ACoFe, A= Na^+, K^+, Rb^+, Cs^+) have been reported.[1,2] The remarkable properties of the latter are due to the photoinduced electron transfer that involves the switching of the Co^{III}-NC-Fe^{II} diamagnetic pairs into the Co^{II}-NC-Fe^{III} paramagnetic ones; this results in a photoinduced magnetic order achieved below a temperature comprised between 15 and 23 K depending on the composition.[1,2] Different types of CNPs based on such PBAs have been reported during the past decade, and in some cases it has been shown that magnetic bistability can be retained below 50 nm, and in a few cases below 10 nm.[7,8d] A major challenge is to go a step further by designing nano-objects where magnetic bistability can be monitored by light; this may be achieved at higher temperatures by creating a synergy. One example of synergy between magnetism and photomagnetism has been reported by Pajerowski et al. on heterostructured films of $K[MCr(CN)_6]/Rb[CoFe(CN)_6]/K[MCr(CN)_6]$ (M = Ni or Co) with a persistent photoinduced decrease of the magnetization up to T_c = 90 K attributed by the authors to canting effects at the interface.[11,12] Synergy can also be achieved in magnetic CNPs using the approach we have pioneered and that consists in the design of core-multishell nano-objects made of one[13] or various[7g−14] PBAs interacting together. In the present paper, we investigate the magnetic and the photomagnetic behavior of nanoparticles made of a ferromagnetic core surrounded by two successive shells: the first one being

Received: February 5, 2013
Published: August 29, 2013

   dx.doi.org/10.1021/ic400303x | *Inorg. Chem.* 2013, 52, 10264−10274

photomagnetic and the second one ferromagnetic (see Scheme 1). The aim is to study the effect of the ferromagnetic components (CsNiCr) on the magnetic behavior of the photosensitive magnetic shell (CsCoFe). During the course of our work, an example of synergy in Rb-based cobalt hexacyanidoferrate (RbCoFe) heterostructures larger than 500 nm has been reported, the preparation of which was based on our procedure[7g] with slight modifications in the particles' isolation.[15] Photoinduced synergetic effects are similar to the above-mentioned multilayered films and give a first illustration of the new behaviors that heterostructured CNPs can present. The present work evidence synergetic effects on PBAs core multishell nanocrystals containing Cs^+ with a size *below 50 nm* (1 order of magnitude smaller than those reported). The core-multishell CNPs were obtained in a seed-mediated multistep procedure that leads *without any isolation* to the precise targeted size with a 10% standard deviation with a full control of the valence states of the iron and cobalt metal ions, which is crucial for reliable correlations between the observed effects. As for bulk compounds[2] the insertion rate of Cs^+ alkali ions in the tetrahedral vacancies of the CoFe shell has a strong influence on the number of diamagnetic pairs that may be photoswitched into paramagnetic pairs. We have examined and compared in the present work related heterostructured CNPs with CoFe shells containing or not containing cesium ions.

The crystallinity, valence states, and magnetic properties of the resulted CNPs were found to be strongly influenced by the presence of Cs^+ ions in the CoFe layer. The preparation of the objects can be summarized as follows; 6 nm negatively charged CsNiCr seeds were grown to reach a size of 12 nm (step 1, compound **1**), followed by the growth of a 10 nm thick either CsCoFe shell or CoFe shell (step 2). In the first series (**2** and **3**), the CoFe shell was grown without any Cs^+ ion and is expected to contain only Co^{II}-NC-Fe^{III} paramagnetic pairs. In the second series (**2Cs** and **3Cs**), Cs^+ ion was introduced during the growth of the CoFe shell and is expected to predominantly yield photoswitchable diamagnetic Co^{III}-NC-Fe^{II} pairs. The final stage (step 3) consists in growing a 5 nm CsNiCr additional shell to reach the 42 nm final objects denoted as **3Cs** or **3** whether they include Cs^+ ion or not.

Scheme 1. Synthetic Strategy and Targeted Core Multishell CNPs[a]

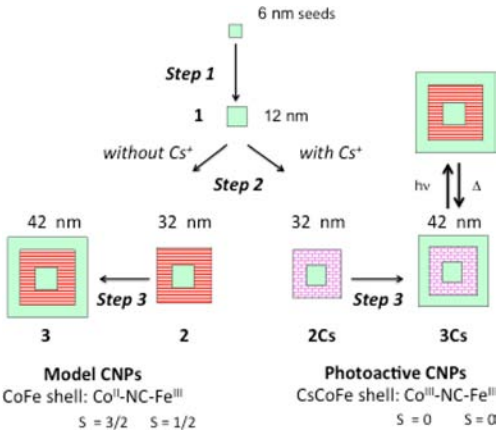

[a]CsNiCr, green; CsCoFe, violet; CoFe, red. The mentioned sizes correspond to the overall diameter of **1**, **2**, **2Cs**, **3**, and **3Cs**.

The irradiation of **2Cs** and **3Cs** may induce the photoinduced electron transfer to lead to the formation of an intermediate CsCoFe shell made of Co^{II}-NC-Fe^{III} paramagnetic pairs. Compounds **2** and **3** will thus be considered as *model compounds* of the photoinduced magnetic behaviors of **2Cs** and **3Cs** *after* irradiation.

Magnetic and photomagnetic measurements on the obtained CNPs revealed two major points; (i) the uniform reversal of the magnetization which is attributed to an efficient exchange coupling leads to enhanced magnetization and coercive field, and (ii) for the first time, the photoinduced *increase* of the magnetization maintained up to 60 K, which corresponds to the ordering temperature[16] of the CsNiCr component, showing that the ferromagnetic components align the magnetization of the photoactive shell.

EXPERIMENTAL DETAILS

All reagents and chemicals were purchased from commercial sources and used without further purification. The synthesis of the core−shell nanoparticles is adapted from the original procedure developed by us.[7g]

Synthesis of 12 nm "Core" $CsNiCr(CN)_6$ [1]. These nanoparticles were synthesized as reported.[13] On 10 mL of the 6.0 ± 0.5 nm seed nanoparticles[7e] in aqueous solution further diluted in 10 mL of distilled water were added dropwise and simultaneously (1 mL min^{-1}) two equal volumes (35 mL) of aqueous solutions of $NiCl_2 \cdot 6H_2O$/CsCl (2 mM; 0.07 mmol/4 mM; 1.4 mmol) and of $K_3Cr(CN)_6$ (2 mM; 0.07 mmol). The solution was kept under vigorous stirring for 1 h after the addition is complete leading to a light green solution of the 12 nm CsNiCr nanoparticles.

Synthesis of 32 nm CsNiCr@CoFe CNPs [2]. Thirty milliliters of the aqueous solution of **1** was diluted in an equal volume of water. Then, acidified aqueous solutions (247 mL; pH = 3) of $CoCl_2 \cdot 6H_2O$ (0.37 mmol; 1.5 mM) and of $K_3[Fe(CN)_6]$ (0.37 mmol; 1.5 mM) were added dropwise and simultaneously under stirring, at room temperature. The rate of addition was kept low (1 mL min^{-1}). The solution turned to the typical brown color of the Co^{II}−Fe^{III} system.

Synthesis of 32 nm CsNiCr@CsCoFe CNPs [2Cs]. As for **2**, 30 mL of the aqueous solution of **1** was diluted in an equal volume of water. A 247 mL portion of an acidified aqueous solution of $CoCl_2 \cdot 6H_2O$ (0.37 mmol; 1.5 mM; pH = 3) and CsCl (0.14 mmol; 0.6 mM) and 247 mL of an acidified aqueous solution of $K_3Fe(CN)_6$ (0.37 mmol; 1.5 mM; pH = 3) were slowly added (dropwise; 1 mL min^{-1}) under stirring. The solution turned to the typical dark purple color of the Co^{III}−Fe^{II} system.

Synthesis of 42 nm CsNiCr@CoFe@CsNiCr [3] and CsNiCr@CsCoFe@CsNiCr [3Cs]. A similar procedure was applied to grow the 5 nm CsNiCr external shell on **2** and **2Cs**. A 100 mL portion of the previously prepared core−shell aqueous solution of **2** (or **2Cs**) was diluted in 100 mL of water, then two equal volumes (59 mL) of aqueous solutions of $NiCl_2 \cdot 6H_2O$ (0.088 mmol; 1.5 mM) with CsCl (0.17 mmol; 3 mM) and of $K_3Cr(CN)_6$ (0.088 mmol; 1.5 mM) were added slowly and simultaneously. The rate of addition was kept low (1 mL min^{-1}) under vigorous stirring at room temperature.

The core-multishell CNPs were then isolated with the following three procedures. (*i*) By adding the aqueous solution of nanoparticles into a 6 mM methanolic solution of cetyltrimethylammonium bromide (CTAB) in a volume ratio MeOH:H_2O = 3, after which the solution of flocculated particles was centrifuged at 8000 rpm during 15 min and the precipitate washed once with water, twice with acetonitrile, and dried under vacuum. The obtained powder was used for all analysis (infrared spectroscopy, X-ray powder diffraction, elemental analysis by energy dispersive X-ray spectroscopy (EDS), transmission electron microscopy (TEM), magnetic measurements). (*ii*) By addition of 100 equiv of polyvinylpyrrolidone (PVP) K40 and precipitation with 3 volumes of acetone (for water solubilization to perform UV−visible spectroscopy). (*iii*) By precipitating particles with a few drops of a saturated solution of zinc chloride; the flocculate was centrifuged,

dx.doi.org/10.1021/ic400303x | *Inorg. Chem.* 2013, 52, 10264−10274

washed with water, and then dried under vacuum; the obtained powder was characterized and used for photomagnetic measurements.

Dynamic light scattering (DLS) and zeta potential measurements were performed on a Malvern Nanozetasizer Apparatus (equipped with a backscattering mode) on 1.5 mL of the as-prepared particles in solution. The volume profile was used to estimate the size of the hydrodynamic diameter.

Fourier transformed-infrared (FT-IR) spectra were collected in the transmission mode on a Perkin-Elmer Spectrum100 spectrometer.

X-ray powder diffraction was performed on thoroughly grown powders deposited on an aluminum plate and the data were collected on a Philipps Panalytical X'Pert Pro MPD powder diffractometer at CuK_α radiation length equipped with a fast detector.

Energy-dispersive X-ray spectroscopy (EDS) was carried out using an IDFix SAMx system installed on a Zeiss Supra 55 FEG-SEM. The high voltage was set at 20 kV, and samples were situated at the optimal working distance. Analyses were performed on powder over a large area to get rid of topographic effects as much as possible, and several analyses were done for each sample.

Scanning transmission electron microscopy experiments were done using a dedicated cold field-emission gun scanning-transmission electron microscope vacuum generator HB05 (FEG STEM VG HB05). High angle annular dark field images were recorded using a collection angle above 60 mrad and an acquisition time of around 15 s per image.

The TEM measurements have been done on a TEM Philips EM208 with 100 keV incident electrons focused on the specimen.

The photomagnetic experiments were performed using a Spectrum Physics Beamlok 2060 laser (λ = 647 nm, P = 3 mW/cm^2) coupled via an optical fiber to the cavity of a MPMS-5S Quantum Design SQUID magnetometer. Samples of **2Cs** and **3Cs** were maintained in a straw between two thin layers of polyethylene films to limit orientation effects. Note that the temperatures have been corrected to take into account the light irradiation heating (an average +2 K has been observed with red light).

RESULTS

Synthesis, Composition, and Size Determination of the Multishell CNPs. A crucial condition to finely control the size of core multi-shell CNPs is to perform the growth on homogeneous seeds. This condition, that limits the homogeneity of many PBA heterostructures,[15,17] is fulfilled for the negatively charged 6 nm CsNiCr particles reported in our group.[7e] This leads to a fine control of larger CsNiCr CNPs by a stepwise addition of the precursors as described recently. The 12 nm size set for the CsNiCr "cores" **1** was targeted as it lies in the magnetic single domain regime.[13] To grow the first and second shells on these cores, the conditions were screened to avoid any side nucleation (dilution of the mother solution, slow addition and low concentrations of precursors' solutions). This was however complicated by the acidic conditions—that increase the ionic strength—required to prevent the formation of Co^{II}-NC-Fe^{II} pairs. The growth of the CsCoFe shell was therefore tested for different amounts of *added* CsCl, and an optimum was found at 0.4 equiv of Cs^+ per cobalt ion (see Supporting Information, Figures S1a and S1b). This has led to a convenient insertion of the alkali ion in the resulting PBA shell (close to 0.5 equiv per cobalt ion, accounting for the additional cesium ions that remained in solution after the preparation of **1**) while preventing side nucleation induced by a higher ionic force (i.e., excess cesium ions in solution). As described on the bulk compound,[2] the insertion of Cs^+ ion in the photomagnetic shell was expected to induce a large amount of photoswitchable Co^{III}-NC-Fe^{II} diamagnetic pairs.

The stepwise growth of the CNPs was followed by dynamic light scattering (DLS). It has revealed a coherent increase of the overall hydrodynamic diameter, with no additional peaks, thus ascertaining that no side nucleation occurs. The starting seed CNPs of CsNiCr have a hydrodynamic diameter of 7 nm. The measured hydrodynamic diameter increases to 15 nm for **1** (12 nm CsNiCr cores), to 32 nm for **2Cs**, and to 43 nm for **3Cs** (Supporting Information, Figure S2). For compounds **2** and **3**, larger hydrodynamic diameters have been observed (50 nm for **2** and 78 nm for **3**, see Supporting Information, Figure S3a) but a coherent increase is nevertheless observed and aggregation was discarded by TEM observations (Supporting Information, Figure S3b). The zeta potentials have been measured on the aqueous suspensions of the CNPs: negative values of −29 mV, −15 mV, −27 mV, and −32 mV have been obtained for **2**, **2Cs**, **3**, and **3Cs**, respectively, explaining the good stability of the CNP solutions, over months.

Nanoparticles have been recovered as powders by addition of either CTAB, where the CTA^+ cation balances the negative charge of the inorganic CNPs, or PVP for subsequent water dispersion.

The four CNPs samples surrounded by CTA^+ have been studied by Infrared (IR) spectroscopy (Figure 1). This technique gives valuable information on the valence state of metal ions in PBAs, especially in the case of CoFe.[1,2] In the 2000−2500 cm^{-1} region, **2** and **3** display a band at 2158 cm^{-1} corresponding to Co^{II}-NC-Fe^{III} bridges as well as a broad band around 2100 cm^{-1} assigned to some reduced Co^{II}-NC-Fe^{II} pairs (2090 cm^{-1}) and a minority of Co^{III}-NC-Fe^{II} units. For samples **2Cs** and **3Cs**, this broad band is observed at 2118 cm^{-1} and is due to the overlapping between a large contribution from the vibration at 2120 cm^{-1} of the predominant Co^{III}-NC-Fe^{II} pairs and the Co^{II}-NC-Fe^{II} vibration at 2097 cm^{-1} (that also overlaps the Ni^{II}-NC-Fe^{II} band of the pairs at the interface). As no band was detected at 2158 cm^{-1}, these two samples have negligible amounts of Co^{II}-NC-Fe^{III} pairs, indicating the successful insertion of Cs^+ ions in the lattice.[18] The weak intensity of the Ni^{II}-NC-Cr^{III} vibrations (expected at 2172 cm^{-1}) in this region can be attributed to a weaker oscillator strength of the chromicyanide than that of the ferricyanide.[19]

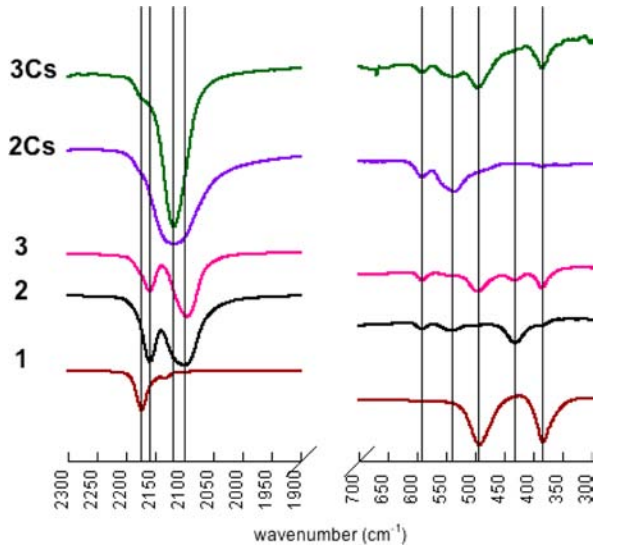

Figure 1. Infrared spectra in the 1900−2300 cm^{-1} and 300−700 cm^{-1} regions for **1** (brown), **2** (black), **3** (light purple), **2Cs** (purple), **3Cs** (green).

dx.doi.org/10.1021/ic400303x | *Inorg. Chem.* 2013, 52, 10264−10274

The low frequency region (200−700 cm^{-1}) also gives important complementary information, as the metal−ligand vibrations that are probed in this region (here metal−carbon of the cyanide) are influenced not only by the nature and the valence of the hexacyanidometalate, but also by the metal coordinated to the nitrogen. The presence of the CsNiCr core and (Cs)CoFe external shell is well evidenced in this region, as the two intense vibrations (metal carbon rocking and elongation modes) at 385 cm^{-1} and 497 cm^{-1} are characteristic of the formation of Ni-NC-Cr bridging entities as shown for **1**. The relative intensity of these peaks significantly increased when going from **2** to **3**, and from **2Cs** to **3Cs**. This clearly demonstrates the growth of the external CsNiCr shell.

Furthermore, the valence state of the CoFe shell is also probed in this spectral range. The presence of $[Fe^{II}(CN)_6]^{4-}$ coordinated to cobalt ions is characterized by metal−carbon bands at 592 cm^{-1} (with Co^{II}) and a broad contribution at 535 cm^{-1} (with Co^{III}), while $[Fe^{III}(CN)_6]^{3-}$ coordinated to cobalt ions gives rise to a metal−carbon vibration at 430 cm^{-1}. These three bands are observed in **2** and **3**, with a predominant one at 430 cm^{-1} that reveals a majority of Co^{II}-NC-Fe^{III} paramagnetic pairs in both **2** and **3**, as expected when a small amount of Cs^+ is inserted. In the case of **2Cs** and **3Cs**, no vibration due to coordinated $[Fe^{III}(CN)_6]^{3-}$ is observed, and the two bands at 591 cm^{-1} and 533 cm^{-1} confirm that Co-NC-Fe^{II} bonds are present. This ascertains that Cs^+ is well inserted in the CoFe shell and favors the electron transfer in **2Cs** and **3Cs** with small amounts of residual Co^{II}-NC-Fe^{III} paramagnetic pairs.[18]

UV−visible spectroscopy has been performed on aqueous dispersions of the compounds surrounded with PVP (CTA^+ samples are not soluble in water) to identify the electronic transitions. The PVP matrix surrounding the particles will limit solvent effects on the charge transfer processes. The violet color of the aqueous solutions of **2Cs** and **3Cs** is characteristic of Co^{III}-NC-Fe^{II} pairs with a broad intervalence band due to the metal-to-metal charge transfer (MMCT) from Fe^{II} to Co^{III} at 550 nm that extends up to 700 nm (Figure 2). Samples **2** and **3** have the brown-red color characteristic of dominant ligand-to-metal charge transfer (LMCT) of coordinated ferricyanide at 390 nm, and a band around 500 nm that may be assigned to a mixture of MMCT and d-d transitions. This is a further evidence of the presence of Co^{II}-NC-Fe^{III} paramagnetic pairs are primarily present at room temperature in samples **2** and **3** for which insertion of alkali ions in the CoFe shell is limited.

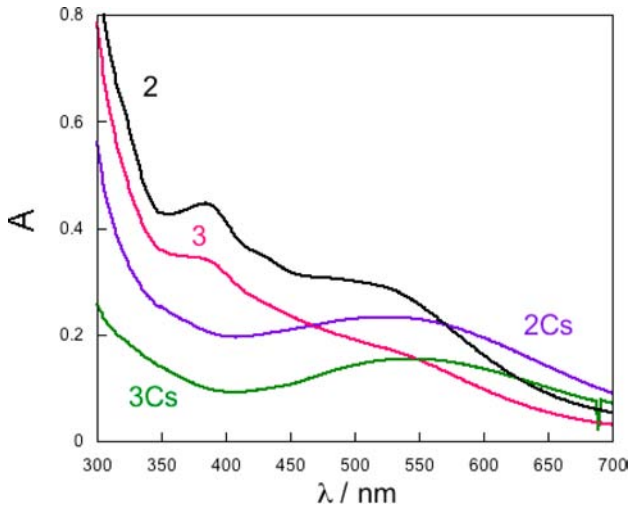

Figure 2. UV−visible absorption spectra of water dispersions of **2**, **3**, **2Cs**, and **3Cs** surrounded by PVP (for a concentration of unit formula of 2.10^{-6} mol L^{-1}).

Transmission electronic microscopy (TEM) has been performed on methanolic dispersions of the particles surrounded by CTA^+. The quality of the dispersion was checked by DLS. TEM has revealed fairly homogeneous particles with a well faceted rectangular prismatic shape with a small anisotropy for **2** and **3**, while a cuboctahedral-like shape is observed for **2Cs** and **3Cs** (Supporting Information, Figure S3b and Figure 3). The mean sizes determined from the size distributions are consistent with the targeted sizes. For the 32 nm target core@shell nanoparticles, the mean size is 32.0(±2.9) nm for **2** (larger dimension 33.2(±2.1) nm) and 35.6(±3.1) nm for **2Cs**. For the core@shell@shell CNPs targeted at 42 nm, a mean size of 42.8(±3.7) nm (larger dimension 46.7(±4.1) nm) is observed for **3** and 42.3(±4.6) nm for **3Cs** (Figure 3). A standard deviation close to 10% is observed on both series. This very good agreement with the targeted size shows that the tailoring of PBA-based heterostructured CNPs can be finely achieved.

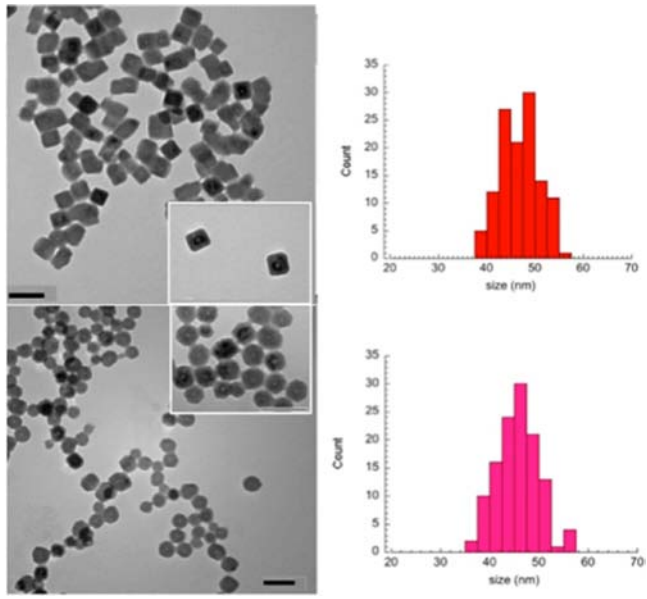

Figure 3. Left: Transmission electronic micrographs of **3** (top, with zoom as inset) and **3Cs** (bottom, with zoom as inset), scale bars = 100 nm. Right: size distribution of **3** (top) and **3Cs** (bottom).

The composition of the four samples has been determined by energy dispersive X-ray spectroscopy (EDS, see Supporting Information, Table S1). The composition of the CsNiCr cores **1** was determined first. Then the compositions of the first and second shells were deduced subsequently. When isolated as powders, the negative charge borne by the inorganic cores is balanced by the presence of cations that are different depending on the recovery process (CTA^+ when using CTAB, Cs^+ for PVP-samples, Zn^{2+} when using $ZnCl_2$). The obtained compositions of the PBA inorganic cores common to all samples correspond to the following formulas:

$\{Cs_{0.5}NiCr_{0.95}@(Cs_{0.1}CoFe_{0.7})_{20}\}$ for **2**

$\{Cs_{0.5}NiCr_{0.95}@(Cs_{0.5}CoFe_{0.8})_{19}\}$ for **2Cs**

dx.doi.org/10.1021/ic400303x | Inorg. Chem. 2013, 52, 10264−10274

$\{Cs_{0.5}NiCr_{0.95}@(Cs_{0.1}CoFe_{0.7})_{20}@(Cs_{0.5}NiFe_{0.1}Cr_{0.7})_{25}\}$ for **3**

$\{Cs_{0.5}NiCr_{0.95}@(Cs_{0.5}CoFe_{0.8})_{19}@(Cs_{0.5}NiFe_{0.1}Cr_{0.7})_{24}\}$ for **3Cs**

The intended 1.34 Ni/Co molar ratio used in the synthesis to achieve the targeted CNPs was confirmed by EDS for **3** and **3Cs** (1.27 and 1.34 respectively see Supporting Information, Table S1).[20]

When performing epitaxial growth of a CoFe shell on top of a CsNiCr core, Ni-NC-Fe and Co-NC-Cr pairs are generated at the interface. In the present case, these analyses show that the composition of the CsCoFe shell in **2Cs** has the expected amount of inserted Cs^+ and 20% vacancies in hexacyanidoferrate, indicating that some $[Fe^{III}(CN)_6]^{3-}$ remains in solution after the growth of the CsCoFe shell. As a consequence, a thin layer of $NiFe(CN)_6$ PBA grows between the CsCoFe shell and the external CsNiCr shell leading to only Ni-NC-Fe pairs at the interface (instead of 50% Ni-NC-Fe and 50% Co-NC-Cr bonds).[18] This interfacial NiFe layer is also observed in **3** as the CoFe shell presents 30% vacancies in $[Fe^{III}(CN)_6]^{3-}$.

The thickness of this layer is estimated to be smaller than 1 nm (2 layers of NiFe) and 1.5 nm (3 layers of NiFe) in the case of compounds **3** and **3Cs** respectively.[21]

Preliminary experiments have shown that, when required, this interfaced layer may be avoided by introducing 20% less ferricyanide in the (Cs)CoFe preparation (Supporting Information, Table S2). In summary, our procedure leads thus to controlled heterostructured objects with a good knowledge of the predominant valence state in the (Cs)CoFe shells.

Structural Characterization and Spectromicroscopy. X-ray powder diffraction (XRD) was performed on all samples to evidence the formation of distinct crystalline shells of the different PBAs in the CNPs (Supporting Information, Figures S4 and S5). The diffractograms of **2Cs** and **3Cs** confirm the presence of both the CsNiCr and the CsCoFe networks each with the expected fcc structures. Figure 4 shows the characteristic peaks of each PBA zoomed on the (400) peak. The cell parameters extracted from the (200), (220), and (400) planes lead to a mean cell parameter of 10.47 Å and 9.94 Å for the CsNiCr and $CsCo^{III}Fe^{II}$ PBAs, respectively, in good agreement with the cell parameters of the corresponding bulks.[2,10] This supports the spectroscopic data (IR and UV–visible) that show the prevalence of Co^{III}-NC-Fe^{II} pairs at room temperature within these compounds.

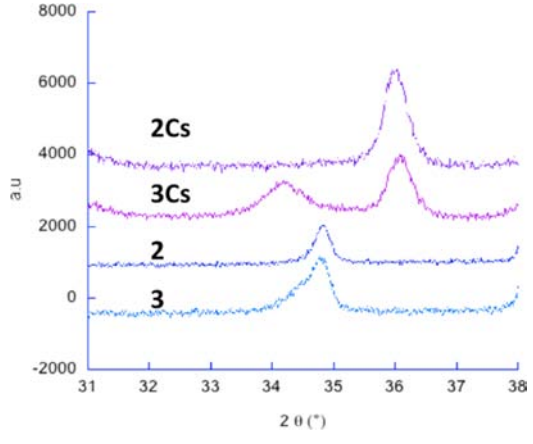

Figure 4. X-ray powder diffraction patterns zoomed on the (400) peaks for **2**, **3**, **2Cs**, and **3Cs**.

Compounds **2** and **3** have different diffraction patterns with apparent slightly asymmetric single peaks. The cell parameter extracted from the peak maxima for compounds **2** and **3** gives a value of 10.30 Å. This is in agreement with dominant Co^{II}-NC-Fe^{III} pairs and the reported cell parameters of the corresponding $Co^{II}Fe^{III}$ PBA bulk compound.[1,2] The asymmetric shape of the peaks in **3** occurs from the overlapping of the CoFe shell diffraction peaks with that of the CsNiCr shell (close to 10.40 Å), evidencing the segregation of the two components.[22]

To gain more insight on the crystallinity of these nanoparticles, high resolution TEM (HRTEM) was performed on both **3** and **3Cs**. Nanocrystals of **3** show very flat surfaces, sometimes atomically flat, and show excellent crystallinity (see also Supporting Information, Figures S6 to S9). However, they present dislocations at the interface and in the shell that relax the strain at the interface. Even if a rough surface is observed for nanoparticles of **3Cs**, they reveal a good crystallinity, with a low number of defects. Dislocations are found at the interfaces that accommodate the large cell parameter difference between the two PBAs (Δa = 0.5 Å), as shown in Figure 5. Despite the very different morphologies, both samples are crystalline.

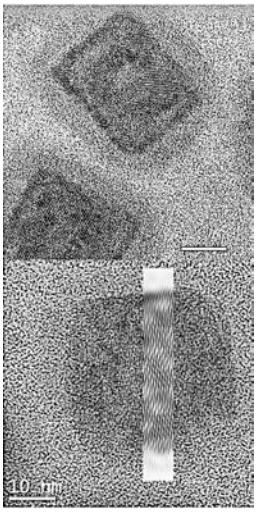

Figure 5. HRTEM images of **3** (top) and **3Cs** (bottom). Scale bars: 10 nm. Lattice fringes are highlighted on **3Cs**.

The local chemical compositions of the nanocrystals were probed by STEM-EELS to further highlight the core–shell structure. This technique establishes the chemical profiles by detecting the characteristic edges of each element, in the present case along a line that crosses the nanoparticle. Because of the roughness of the surface and their cuboctahedral shape, the nanoparticles of **3Cs** were not well aligned with respect to the grid plane, so that the profiles (Figure 6, top and middle) appear more uneven than for **3**.[23]

Nevertheless, each profile indicates the targeted heterostructure for both CNPs, with Cr located in the core and in the external shell, while Fe is located in the intermediate layer (Figure 6 top and middle left); moreover, the composition in Cs and in N from the cyanides is uniform over the whole particle in **3Cs** (Figure 6 top right) while in **3** a deficiency in Cs

dx.doi.org/10.1021/ic400303x | Inorg. Chem. 2013, 52, 10264–10274

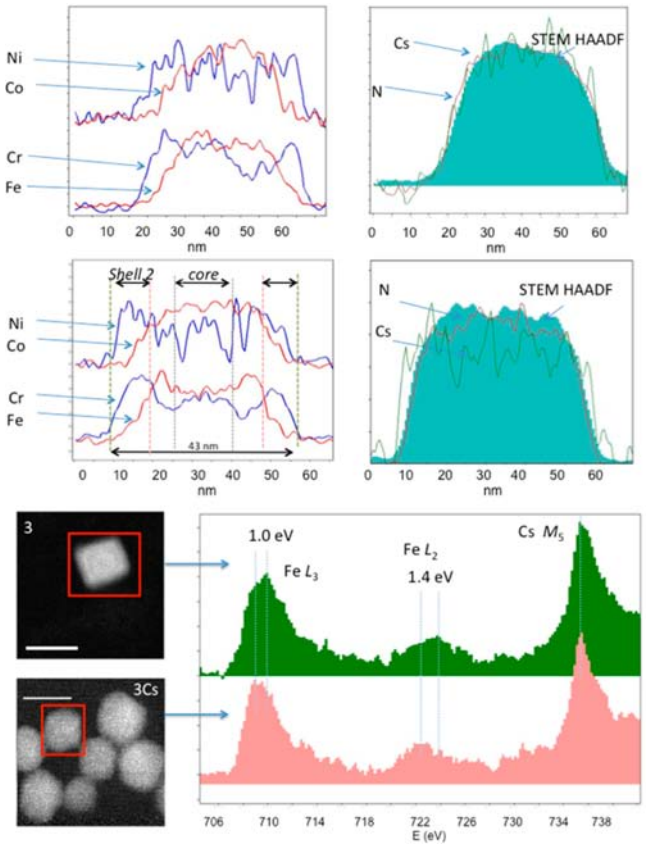

Figure 6. Top and middle: STEM-EELS profile (left Ni, Co, Cr, Fe, right: N and Cs red line) of **3Cs** (top) and **3** (middle). Bottom: HAADF images and zoom on the Fe L_2 and L_3 edges detected by EELS of **3** (top) and **3Cs** (bottom).

(Figure 6 middle right) is, as expected, observed in the intermediate shell (still it is nonzero since the external shell is probed simultaneously). The valence states of the iron ions were further probed on the Fe $L_{2,3}$ edge features (Figure 6 bottom). While **3Cs** contained mainly Fe^{II} (Co^{III}-NC-Fe^{II} and Co^{II}-NC-Fe^{II} pairs), **3** contains about 70% Fe^{III} (Co^{II}-NC-Fe^{III} pairs) and about 30% of Fe^{II}.

This is in good agreement with the other spectroscopic data confirming a majority of Co^{II}-NC-Fe^{III} paramagnetic pairs for **3**, while Co^{III}-NC-Fe^{II} photomagnetic pairs are mainly present in **3Cs.**

Magnetic and Photomagnetic Experiments. As they primarily contain paramagnetic $Co^{II}Fe^{III}$ pairs the study of samples **2** and **3** (surrounded by CTA^+) is highly relevant since they represent models of the magnetic behavior expected after full photoconversion of the diamagnetic $Co^{III}Fe^{II}$ pairs contained in the parent CNPs **2Cs** and **3Cs**. Zero-field cooled (ZFC) and field cooled (FC) magnetizations measured from 100 to 5 K are presented in Figure 7. The ZFC magnetization curve of **2** shows a broad maximum around 25 K with a sharper peak at 19 K, and the FC/ZFC magnetization curves converge at 38 K. The broad contribution at 25 K is attributed to the single-domain 12 nm CsNiCr cores. These particles, when fully isolated by PVP, exhibit a broad maximum of the ZFC magnetization around 17 K.[13] In **2** despite a large inter-cores separation (i.e., twice the CoFe shells of 10 nm that are paramagnetic above 20 K and the double CTA^+ layers), some dipolar interactions occur between the ferromagnetic CsNiCr single-domain cores and raise slightly the ordering temperature.[16] Below 20 K, the proximity of the 10 nm thick CoFe shells in **2** leads to strong interparticle dipolar interactions through the CTA^+ layers, that are responsible for the magnetic ordering[16] observed at 19 K, close to that of the bulk CoFe. For **3**, the presence of an additional external CsNiCr shell leads to a large signal below 60 K (at which temperature the ZFC and the FC converge) and a weaker maximum at 14 K. This evidences the presence of the magnetic ordering (either ferrimagnetic order or spin glass-like behavior) of the $Co^{II}Fe^{III}$ shell (around 14 K) in addition to that of the CsNiCr (below 60 K) that results from strong dipolar interactions between the nanoparticles. For the 5 nm CsNiCr external shell this temperature is smaller than that observed on the bulk (90 K) which can be due to (i) a large proportion of sites located on the surface and on the interfaces that reduces the average number of Ni and Cr neighbors, and (ii) weakened interparticle interactions resulting from the presence of CTA^+.

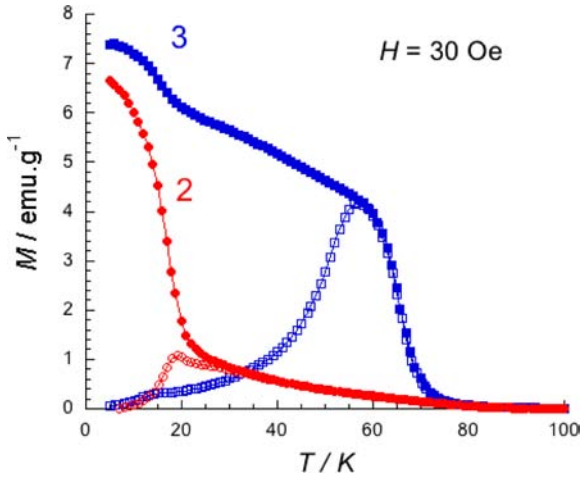

Figure 7. Field cooled (full symbols) and zero-field cooled (open symbols) magnetizations under a field of 30 Oe for samples **2** (circles) and **3** (squares), at a sweeping rate of 1 K min^{-1}.

The intensity of the two maxima is related to the proportion of each component (Ni/Co = 1.34) along with the stronger spin value of the CsNiCr PBA due to ferromagnetic interactions between Ni^{II} and Cr^{III} (S_{Ni}^{II} = 1 and S_{Cr}^{III} = 3/2; S_{NiCr} = 5/2), while the $Co^{II}Fe^{III}$ PBA shows antiferromagnetic interactions between *high-spin*-Co^{II} and *low-spin*-Fe^{III} (S_{Co}^{II} = 3/2 and S_{Fe}^{III} = 1/2; S_{CoFe} = 1). The field dependence of the magnetizations measured between −0.8 and 0.8 T for compounds **2** and **3** are shown in Figure 8.

Both compounds exhibit a hysteresis loop with a uniform reversal of the magnetization, when the particles are blocked in eicosane. Coercive fields of 1500 and 1000 Oe are measured for **2** and **3**, with reduced remanent magnetizations $M/M_{saturation}$ close to 0.5. When the particles were studied without eicosane, strong orientation effects were easily observed by the presence of a zero field step in the hysteresis.[24]

Magnetic studies were performed before and after irradiation of samples **2Cs** and **3Cs** with a red light (λ = 647 nm) in the SQUID. During the irradiation at 10 K under an applied field of 30 Oe, a continuous increase of the magnetization is observed until a steady state is reached after 5 h, because of the photoinduced electron transfer that provokes the switching of the diamagnetic Co^{III}-NC-Fe^{II} pairs (S = 0) into the paramagnetic Co^{II}-NC-Fe^{III} (S = 1) pairs within the CsCoFe shell.

dx.doi.org/10.1021/ic400303x | *Inorg. Chem.* 2013, 52, 10264−10274

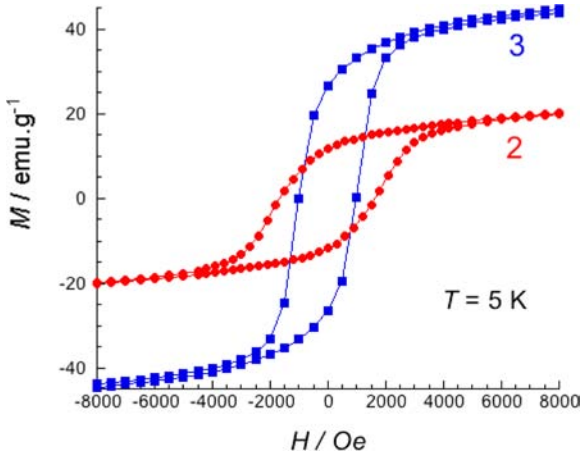

Figure 8. Magnetization versus field for samples **2** (red) and **3** (blue) at T = 5 K.

The hysteresis curves $M = f(H)$ measured before and after irradiation have a peculiar shape for **2Cs**, with a small step at zero field (Figure 9) that was not observed on the model

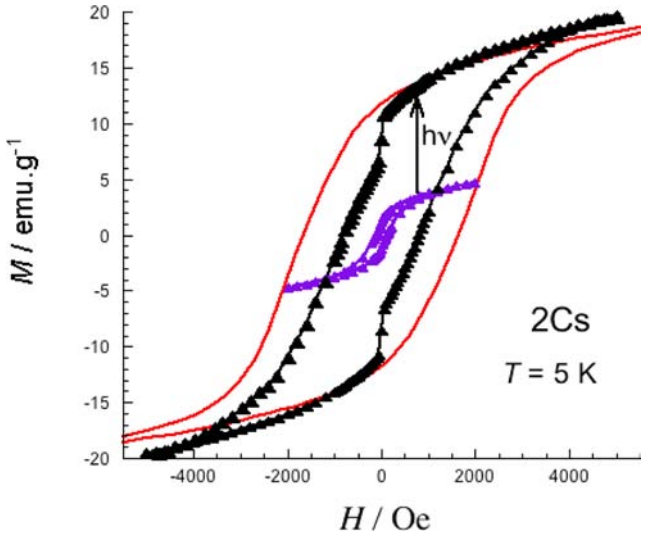

Figure 9. Magnetization versus field at T = 5 K of **2Cs** before irradiation (purple), after irradiation (black); the red curve corresponds to the $M = f(H)$ curve for the "model" compound **2**.

compound **2**. This feature was tentatively attributed to partial reorientation effects in the sample under field that are however lost when the field is almost nil. This type of zero-field step was systematically observed on **2** and **3** when the powders were not blocked in eicosane. For irradiation purposes, such a preparation is obviously not convenient; we have thus tried to limit the orientation by blocking the powder between two plastic films (with tape), and the curve presented in Figure 9 corresponds to the best set of data we could obtain.

Before irradiation, a coercive field of 120 Oe is measured for **2Cs** that increases to 850 Oe after irradiation and becomes of the same magnitude than that reported for bulk compounds,[1] together with a large increase of the magnetization (multiplied by a factor of 3.8) that corresponds to a 45% photoconversion of the diamagnetic pairs according to the composition. It remains smaller than that for compound **2** which is probably due to some partial reorientation of the sample. The initial behavior is fully recovered after heating **2Cs** at 140 K.

The ZFC/FC magnetizations of **2Cs** measured before and after irradiation are plotted in Figure 10. Before irradiation, the

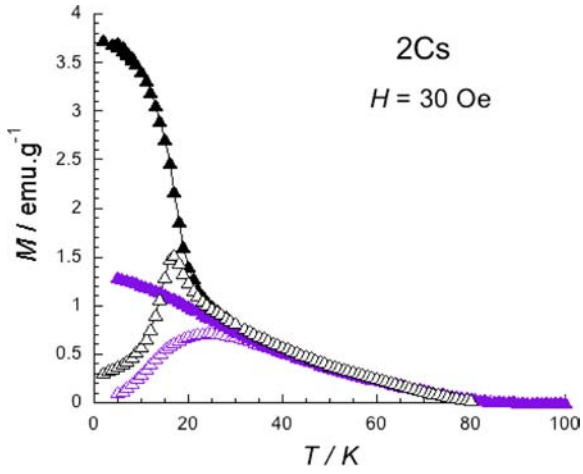

Figure 10. Field-cooled (full triangles) and zero-field cooled (open triangles) magnetizations of sample **2Cs** before irradiation (purple) and after irradiation (black) under a magnetic field of 30 Oe.

ZFC curve shows a broad maximum at 24 K that comes from the single-domain CsNiCr cores weakly interacting through the nearly diamagnetic CoFe shell (composed mainly of Co^{III}-NC-Fe^{II} pairs and of some Co^{II}-NC-Fe^{II} pairs). After irradiation at 10 K, the ZFC/FC magnetizations change drastically because of the onset of a ferrimagnetic order below 17 K. The phototransformation of **2Cs** leads to ZFC/FC magnetizations curves which behavior is similar in shape to that of the model compound **2** (Figure 7). This clearly demonstrates that an efficient phototransformation occurs for cobalt hexacyanidoferrate containing Cs^+ as the inserted alkali ion.

The photomagnetic properties of **3Cs** have been studied for two samples: nanoparticles recovered by CTA^+ (see Supporting Information, Figure S10) or by Zn^{2+} cations. The behaviors were similar except that for the latter orientation effects under field were suppressed as we comment below.

Before irradiation, a hysteresis loop is observed for **3Cs** with a rather high coercive field of 400 Oe. This value is high since the external shell contains only CsNiCr (soft magnet with H_c < 200 Oe even for large nanoparticles[13]) and it may be attributed to the presence of pairs (mainly ferromagnetic Ni^{II}-NC-Fe^{III} pairs[18]) at the interface between the CsCoFe and the CsNiCr shells, or to some local distorsions (because of small changes of cell parameters) around the Co^{II} and Ni^{II} ions that may influence the overall magnetic anisotropy. After irradiation, the coercive field increases to 500 Oe, smaller than that of the model compound **3** (1000 Oe). Importantly, as observed for the model compound, a coherent reversal is observed for **3Cs** with no step at zero field (thus discarding any orientation effect). After irradiation, the photoinduced increase can be seen on the resultant saturation magnetization of the first magnetization curve (Figure 11).

Considering the composition (Ni/Co = 1.34), a 24% increase of the magnetization at saturation is expected after irradiation if all the cobalt ions are considered as Co^{III} and assumed to transform into Co^{II} ions. After irradiation, a 7% enhancement of the saturation magnetization is observed at 5 T

dx.doi.org/10.1021/ic400303x | Inorg. Chem. 2013, 52, 10264−10274

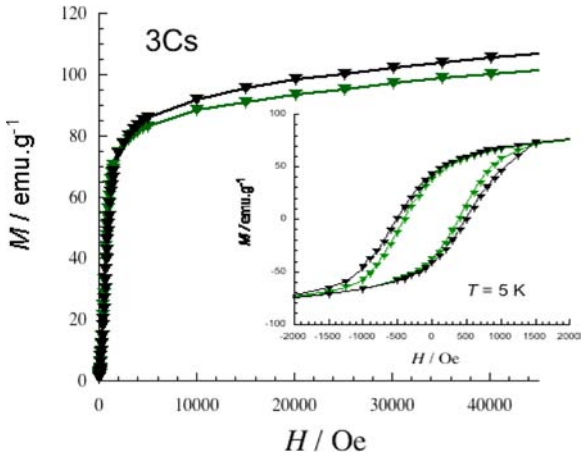

Figure 11. First magnetization versus field at T = 5 K for sample **3Cs** before irradiation (green) and after irradiation (black). Inset: hysteresis curves before and after irradiation.

and corresponds only to a partial conversion (25%) of the CsCoFe shell.

The FC/ZFC magnetizations of **3Cs** have been measured before and after irradiation, as well as after thermal treatment at 140 K (Figure 12).

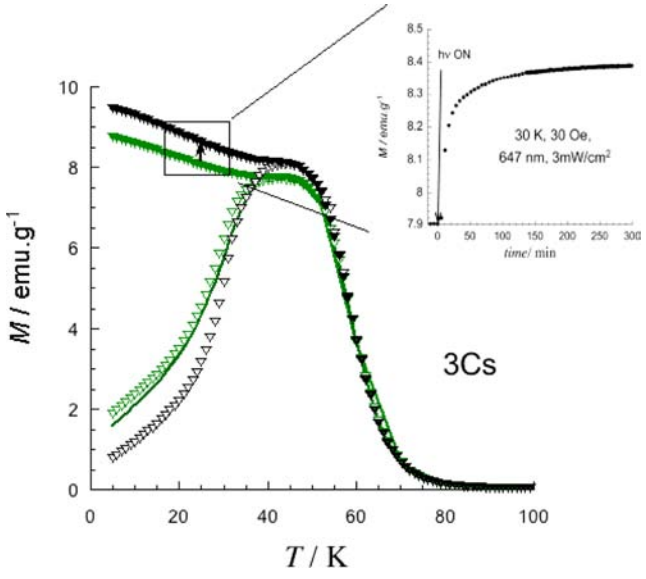

Figure 12. Zero-field cooled (ZFC, open symbols) and field-cooled (FC, full symbols) magnetizations under an applied field of 30 Oe for **3Cs** before irradiation (green), after irradiation (black) and thermal treatment at 140 K (green line). Inset: photoinduced kinetic evolution during irradiation at 30 K under an applied field of 30 Oe.

The signal was first measured under a 30 Oe applied field before applying light and remained constant, discarding then any orientation effects under applied field. No clear maximum is observed on the ZFC magnetization around 14 K as it was observed for model compound **3**. This is probably due to the incomplete phototransformation of the Co^{III}-NC-Fe^{II} pairs that prevents the onset of a clear magnetic ordering.[16] A striking feature here is that the photoinduced magnetic increase of 8% observed at 30 Oe (similar to the increase in the saturation magnetization observed at 5 T) is maintained up to the "ordering" temperature[16] of the ferromagnetic CsNiCr PBA (60 K here, also plotted on Supporting Information, Figure S11).

This behavior is opposite to that observed on thin films and heterostructures above 500 nm,[11,12,15] where a persistent *decrease* of 10−15% of the magnetization is systematically observed. This unprecedented behavior was obtained after irradiation at 10 K and also after irradiation at 30 K that is above the ordering temperature[16] of the CoFe PBA (Figure 11). This unique behavior is fully reversible by heating the compound at 140 K and is also fully reproducible by cycling the irradiation process.

DISCUSSION

Influence of the Cs^+ Insertion. This work aimed at producing core multishell heterostructured CNPs below 50 nm with shells of width thinner than 10 nm by a one-pot procedure. One considerable problem to overcome is the control of both the growth and the composition of the CoFe intermediate shell: (i) on one side to form a large number of Co^{II}-NC-Fe^{III} pairs in the model compounds **2** and **3**, and (ii) on the other side to favor a high number of diamagnetic photoswitchable Co^{III}-NC-Fe^{II} pairs in compounds **2Cs** and **3Cs**. For the latter series this was successfully achieved in growing a Cs-containing CoFe shell since Cs^+ inserts at rather low ionic concentrations hence avoiding nanoparticle aggregation. The addition conditions were yet optimized since CsCoFe is very insoluble and can easily lead to homogeneous nucleation. All spectroscopic data and EDS analysis indicate that the targeted systems were achieved. In **2Cs** and **3Cs**, a Co^{III}-NC-Fe^{II} main valence state is obtained without any residual Co^{II}-NC-Fe^{III} pairs; the presence of ferricyanide vacancies in these compounds has induced an incomplete electron transfer, hence the remaining Co(II) ions and the occurrence of Co^{II}−CN-Fe^{II} pairs. In **2** and **3**, a predominant presence of Co^{II}-NC-Fe^{III} was well evidenced when growing the intermediate shell, as a consequence of the very small content of Cs^+.

A second consequence of the presence of Cs^+ in **2Cs** and **3Cs** is observed on the heteroepitaxial growth of the CsCoFe shell. A CsCoFe PBA is characterized by a cell parameter of 9.95 Å and thus differs significantly from the CsNiCr PBA contained in the core and in the external shell of our objects (Δa = 0.5 Å). For **2** and **3** the divergence is less significant since the $Co^{II}Fe^{III}$ PBA has a cell parameter of 10.35 Å (Δa = 0.15 Å). This can explain the differences in shape observed for the nanocrystals with well faceted CNPs in the case of **3**, while rougher surfaces are obtained for the cubooctahedral-like **3Cs**. However, based on the HRTEM and the XRD data, both systems are crystalline, with the presence of some dislocations that relax the strain at the interfaces and that can also be attributed to the presence of NiFe pairs at the interface. For both systems the multishell structure of the nanocrystals has been further evidenced by spectromicroscopy.

Magnetic and Photomagnetic Properties. *Field Dependence of the Magnetization.* Heterostructured CNPs **2** and **3** may be considered as coordination-based exchange-spring models.[25] They combine in intimate contact a soft (H_c < 100 Oe) ferromagnetic CsNiCr core (and shell for **3**) with a harder magnetic CoFe shell (up to 1500 Oe). Indeed, a uniform reversal of the magnetization (without steps) is observed for both compounds showing the efficient exchange coupling between the two networks. The difference in coercive field values (from 1500 Oe for **2** to 1000 Oe for **3**) is due to the

dx.doi.org/10.1021/ic400303x | Inorg. Chem. 2013, 52, 10264−10274

increased proportion of the softer CsNiCr PBA in **3** that results in a proportional decrease of the coercive field as described on other exchange-coupled nanoparticles.[13,25] Moreover, the large magnetic moment borne by the CsNiCr pairs ($S = 5/2$) along with the $Co^{II}Fe^{III}$ pairs ($S = 1$) leads to nanoparticles that overall combine a large resultant magnetic moment with a large coercive field. With a ratio of 1.34 between the CsNiCr and the CoFe components in **3**, it is thus possible to increase the saturation magnetization by a factor of 3 while the coercive field is multiplied by more than 10 when compared to that of 30 nm pure CsNiCr particles.[13] An exchange coupling is also observed on compound **3Cs** after irradiation, with a uniform reversal of the magnetization. A rather large coercive field is already observed before irradiation, and the small increase of the coercive field after irradiation results from the weak photo-transformation that takes place and thus prevents the onset of a clear ferrimagnetic order in the CsCoFe shell. The moderate increase (7%) of the overall saturation magnetization after phototransformation is also explained by the limited conversion of the switchable pairs in the CsCoFe shell, 25%, half the rate observed in compound **2Cs**. This lower conversion rate may be attributed to a weak light penetration and/or to some strains that impede a complete volume change in the compound. The first eventuality can be discarded by processing the hetero-structures as films to enhance the phototransformation.[26] This approach is currently under progress, and a strong photo-induced exchange-spring mechanism is expected to take place.

Temperature Dependence of the Magnetization. The ZFC and FC magnetizations of **2** and of compound **2Cs** obtained after irradiation are much alike, showing that the model compound **2** and the irradiated **2Cs** behave similarly. This is consistent with the coexistence of two behaviors: a ferrimagnetic ordering of the $Co^{II}Fe^{III}$ shells below 20 K (maximum of the ZFC at 19 K for **2** and 17 K for **2Cs** after irradiation) and the presence of weak interparticle dipolar interactions between the CsNiCr single-domain ferromagnetic cores occurring through the paramagnetic CoFe shells (above 20 K). The comparison of the two sets of FC/ZFC curves also demonstrates the good phototransformation that can be achieved in a CsCoFe shell as the photoconversion here, 45%, matches the rate reported on bulk compounds.[2] Moreover, these results show that 32 nm particles (with a 10 nm CoFe shell) in dipolar interaction through CTA^+ lead to a ferrimagnetic order with a critical temperature close to that reported for the bulk compounds (made of particles larger than 100 nm).[2h]

The ZFC and FC magnetizations of compound **3** reveal also the coexistence of two ordering temperatures associated to the ferrimagnetic CoFe shells and to the ferromagnetic CsNiCr shells being in strong dipolar interaction, at 15 and 60 K respectively.

Lastly, a unique behavior has been observed on compound **3Cs**. The magnetic increase measured at low field (30 Oe) and low temperature (10 K) during the irradiation experiment is observed after irradiation on both the ZFC and the FC magnetizations and persists up to 60 K. This persistent enhancement of the magnetization is the opposite of the behavior described on heterostructured films and large nanoparticles (>450 nm), where a persistent decrease in the FC magnetization was reported.[11,12,15] In our case, another difference appears: the lack of clear ordering of the CsCoFe shell below 15 K, which certainly results from the incomplete phototransformation. Indeed this weak photoconversion leads to the formation of scattered paramagnetic Co^{II}-NC-Fe^{III} pairs within the CsCoFe shell with no large ferrimagnetic domains being formed. The photoinduced response has a similar magnitude at both low and high fields (5 T), and thus cannot be attributed to the effect of the external magnetic field. The pinning of the Co^{II} and Fe^{III} moments that could come from the formation of ferromagnetic Co^{II}-NC-Cr^{III} pairs at the interface between the CsCoFe and the CsNiCr may be discarded here since this interface contains a large majority of Ni-NC-Fe pairs. We can then attribute this magnetization enhancement to the high local magnetic field induced by the ordered CsNiCr ferromagnetic shell that is aligned during the field-cooling process and adds to the external field. This effect vanishes far from the interface between the CsNiCr/CsCoFe shells and may then be neglected in the reported thicker heterostructures, where strain and canting effects dominate the magnetic behavior. These results show that the design and the preparation of ultrathin heterostructures below 50 nm with well-defined sizes and interfaces lead to new synergetic effects.

■ CONCLUSIONS

Photomagnetic/magnetic core multishell nanocrystals with a mean size below 50 nm have been synthesized with a good 10% size control by a one-pot procedure in water. Spectroscopic and structural characterizations have shown the influence of Cs^+ on the morphology and on the valence states of the hetero-structures. The photomagnetic properties of the designed nanocrystals show a uniform reversal of the magnetization characteristic of exchange-spring systems, with a higher magnetization value and a higher coercive field. Importantly, the photoinduced increase of the FC magnetization is maintained up to the ordering temperature (60 K) of the ferromagnetic PBA. This unique synergy stems from the local field effect generated by the ferromagnetic shell on the photoinduced paramagnetic pairs; our results together with those reported on thicker CNPs suggest that such synergetic effects strongly depend on the thickness of the photoactive shells. Efforts to enhance the magnitude of this photoinduced increase are under investigation with the design of ultrathin multishell nanocrystals.

■ ASSOCIATED CONTENT

Ⓢ Supporting Information

Additional comments on the synthesis of **2Cs** and **3Cs**. Further details are given in Figures S1−S11 and Tables S1 and S2. This material is available free of charge via the Internet at http://pubs.acs.org.

■ AUTHOR INFORMATION

Corresponding Author

*E-mail: laure.catala@u-psud.fr (L.C.), mathon@icmcb-bordeaux.cnrs.fr (C.M.), laurent.lisnard@upmc.fr (L.L.).

Notes

The authors declare no competing financial interest.

■ ACKNOWLEDGMENTS

We thank the Université Paris Sud 11, the CNRS (Centre National de la Recherche Scientifique), the French programme ANR-blanc (project MS-MCNP no. 30615), the Institut Universitaire de France (IUF), the Lebanese CNRS, and the Université Libanaise for their financial support.

REFERENCES

(1) (a) Gu, Z. Z.; Sato, O.; Iyoda, T.; Hashimoto, K.; Fujishima, A. *J. Phys. Chem.* **1996**, *100*, 18289−18291. (b) Sato, O.; Iyoda, T.; Fujishima, A.; Hashimoto, K. *Science* **1996**, *272*, 704−705. (c) Sato, O.; Einaga, Y.; Iyoda, T.; Fujishima, A.; Hashimoto, K. *J. Phys. Chem. B* **1997**, *101*, 3903−3905. (d) Sato, O.; Einaga, Y.; Iyo-da, T.; Fujishima, A.; Hashimoto, K. *J. Electrochem. Soc.* **1997**, *144*, L11−L13.

(2) (a) Bleuzen, A.; Lomenech, C.; Escax, V.; Villain, F.; Varret, F.; Cartier dit Moulin, C.; Verdaguer, M. *J. Am. Chem. Soc.* **2000**, *122*, 6648−6652. (b) Cartier dit Moulin, C.; Villain, F.; Bleuzen, A.; Arrio, M. A.; Sainctavit, P.; Lomenech, C.; Escax, V.; Baudelet, F.; Dartyge, E.; Gallet, J. J.; Verdaguer, M. *J. Am. Chem. Soc.* **2000**, *122*, 6653−6658. (c) Champion, G.; Escax, V.; Cartier dit Moulin, C.; Bleuzen, A.; Villain, F. O.; Baudelet, F.; Dar-tyge, E.; Verdaguer, M. *J. Am. Chem. Soc.* **2001**, *123*, 12544−12546. (d) Escax, V.; Bleuzen, A.; Cartier dit Moulin, C.; Villain, F.; Goujon, A.; Varret, F.; Verdaguer, M. *J. Am. Chem. Soc.* **2001**, *123*, 12536−12543. (e) Escax, V.; Champion, G.; Arrio, M. A.; Zacchigna, M.; Cartier dit Moulin, C.; Bleuzen, A. *Angew. Chem., Int. Ed.* **2005**, *44*, 4798−4801. (f) Bleuzen, A.; Marvaud, V.; Mathonière, C.; Sieklucka, B.; Verdaguer, M. *Inorg. Chem.* **2009**, *48*, 3453−3466. (g) Le Bris, R.; Cafun, J. D.; Mathonière, C.; Bleuzen, A.; Létard, J. F. *New J. Chem.* **2009**, *33*, 1255−1261. (h) Cafun, J. D.; Champion, G.; Arrio, M. A.; Cartier dit Moulin, C.; Bleuzen, A. *J. Am. Chem. Soc.* **2010**, *132*, 11552−11559.

(3) (a) Gutlich, P.; Hauser, A. *Coord. Chem. Rev.* **1990**, *97*, 1−22. (b) Kahn, O.; Martinez, C. J. *Science* **1998**, *279*, 44−48. (c) Hauser, A.; Jeftic, J.; Romstedt, H.; Hinek, R.; Spiering, H. *Coord. Chem. Rev.* **1999**, *192*, 471−491.

(4) (a) Niel, V.; Martinez-Agudo, J. M.; Munoz, M. C.; Gaspar, A. B.; Real, J. A. *Inorg. Chem.* **2001**, *40*, 3838−3839. (b) Bonhommeau, S.; Molnar, G.; Galet, A.; Zwick, A.; Real, J. A.; McGarvey, J. J.; Bousseksou, A. *Angew. Chem., Int. Ed.* **2005**, *44*, 4069−407. (c) Bonhommeau, S.; Guillon, T.; Daku, L. M. L.; Demont, P.; Costa, J. S.; Létard, J. F.; Molnar, G.; Bousseksou, A. *Angew. Chem., Int. Ed.* **2006**, *45*, 1625−1629.

(5) (a) Ohkoshi, S.-i.; Arai, K. I.; Sato, Y.; Hashimoto, K. *Nat. Mater.* **2004**, *3*, 857−861. (b) Hashimoto, K.; Kosaka, W.; Nomura, K.; Ohkoshi, S.-i. *J. Am. Chem. Soc.* **2005**, *127*, 8590−8591. (c) Hozumi, T.; Hashimoto, K.; Ohkoshi, S.-i. *J. Am. Chem. Soc.* **2005**, *127*, 3864−3869. (d) Nuida, T.; Hozumi, T.; Kosaka, W.; Sakurai, S.; Ikeda, S.; Matsuda, T.; Tokoro, H.; Hashimoto, K.; Ohkoshi, S.-i. *Polyhedron* **2005**, *24*, 2901−2905. (e) Ohkoshi, S.-i.; Tokoro, H.; Hashimoto, K. *Coord. Chem. Rev.* **2005**, *249*, 1830−1840. (f) Ohkoshi, S.-i.; Ikeda, S.; Hozumi, T.; Kashiwagi, T.; Hashimoto, K. *J. Am. Chem. Soc.* **2006**, *128*, 5320−5321. (g) Ohkoshi, S.-i.; Tokoro, H.; Hozumi, T.; Zhang, Y.; Hashimoto, K.; Mathonière, C.; Bord, I.; Rombaut, G.; Verelst, M.; Cartier dit Moulin, C.; Villain, F. *J. Am. Chem. Soc.* **2006**, *128*, 270−277. (h) Tokoro, H.; Matsuda, T.; Nuida, T.; Moritomo, Y.; Ohoyama, K.; Dangui, E. D. L.; Boukheddaden, K.; Ohkoshi, S.-i. *Chem. Mater.* **2008**, *20*, 423−428.

(6) (a) Tokoro, H.; Ohkoshi, S.-i. *Dalton Trans.* **2011**, *40*, 6825−6833. (b) Ohkoshi, S.-i.; Tokoro, H. *Acc. Chem. Res.* **2012**, *45*, 1749−1758.

(7) (a) Catala, L.; Gacoin, T.; Boilot, J. P.; Rivière, E.; Paulsen, C.; Lhotel, E.; Mallah, T. *Adv. Mater.* **2003**, *15*, 826−827. (b) Uemura, T.; Kitagawa, S. *J. Am. Chem. Soc.* **2003**, *125*, 7814−7815. (c) Uemura, T.; Ohba, M.; Kitagawa, S. *Inorg. Chem.* **2004**, *43*, 7339−7345. (d) Arai, M.; Miyake, M.; Yamada, M. *J. Phys. Chem. C* **2008**, *112*, 1953−1962. (e) Brinzei, D.; Catala, L.; Louvain, N.; Rogez, G.; Stéphan, O.; Gloter, A.; Mallah, T. *J. Mater. Chem.* **2006**, *16*, 2593−2599. (f) Brinzei, D.; Catala, L.; Rogez, G.; Gloter, A.; Mallah, T. *Inorg. Chim. Acta* **2008**, *361*, 3931−3936. (g) Catala, L.; Brinzei, D.; Prado, Y.; Gloter, A.; Stéphan, O.; Rogez, G.; Mallah, T. *Angew. Chem., Int. Ed.* **2009**, *48*, 183−187. (h) Catala, L.; Gloter, A.; Stéphan, O.; Rogez, G.; Mallah, T. *Chem. Commun.* **2006**, 1018−1020. (i) Chelebaeva, E.; Guari, Y.; Larionova, J.; Trifonov, A.; Guerin, C. *Chem. Mater.* **2008**, *20*, 1367−1375. (j) Folch, B.; Guari, Y.; Larionova, J.; Luna, C.; Sangregorio, C.; Innocenti, C.; Caneschi, A.; Guerin, C. *New J. Chem.* **2008**, *32*, 273−282. (k) Kosaka, W.; Tozawa, M.; Hashimoto, K.; Ohkoshi, S.-i. *Inorg. Chem. Commun.* **2006**, *9*, 920−922.

(8) (a) Moore, J. G.; Lochner, E. J.; Ramsey, C.; Dalal, N. S.; Stiegman, A. E. *Angew. Chem., Int. Ed.* **2003**, *42*, 2741−2743. (b) Catala, L.; Mathonière, C.; Gloter, A.; Stéphan, O.; Gacoin, T.; Boilot, J. P.; Mallah, T. *Chem. Commun.* **2005**, 746−748. (c) Taguchi, M.; Yamada, K.; Suzuki, K.; Sato, O.; Einaga, Y. *Chem. Mater.* **2005**, *17*, 4554−4559. (d) Brinzei, D.; Catala, L.; Mathonière, C.; Wernsdorfer, W.; Gloter, A.; Stéphan, O.; Mallah, T. *J. Am. Chem. Soc.* **2007**, *129*, 3778−3779. (e) Fornasieri, G.; Bleuzen, A. *Angew. Chem., Int. Ed.* **2008**, *47*, 7750−7752. (f) Fornasieri, G.; Aouadi, M.; Durand, P.; Beaunier, P.; Rivière, E.; Bleuzen, A. *Chem. Commun.* **2010**, *46*, 8061−8063.

(9) (a) Coronado, E.; Galan-Mascaros, J. R.; Monrabal-Capilla, M.; Garcia-Martinez, J.; Pardo-Ibanez, P. *Adv. Mater.* **2007**, *19*, 1359−1361. (b) Forestier, T.; Mornet, S.; Daro, N.; Nishihara, T.; Mouri, S.; Tanaka, K.; Fouche, O.; Freysz, E.; Létard, J. F. *Chem. Commun.* **2008**, 4327−4329. (c) Gaspar, A. B.; Boldog, I.; Martinez, V.; Pardo-Ibanez, P.; Ksenofontov, V.; Bhattacharjee, A.; Gutlich, P.; Real, J. A. *Angew. Chem., Int. Ed.* **2008**, *47*, 6433−6437. (d) Larionova, J.; Salmon, L.; Guari, Y.; Tokarev, A.; Molvinger, K.; Molnar, G.; Bousseksou, A. *Angew. Chem., Int. Ed.* **2008**, *47*, 8236−8240. (e) Volatron, F.; Catala, L.; Rivière, E.; Gloter, A.; Stephan, O.; Mallah, T. *Inorg. Chem.* **2008**, *47*, 6584−6586. (f) Forestier, T.; Kaiba, A.; Pechev, S.; Denux, D.; Guionneau, P.; Etrillard, C.; Daro, N.; Freysz, E.; Létard, J. F. *Chem.—Eur. J.* **2009**, *15*, 6122−6130. (g) Galan-Mascaros, J. R.; Coronado, E.; Forment-Aliaga, A.; Monrabal-Capilla, M.; Pinilla-Cienfuegos, E.; Ceolin, M. *Inorg. Chem.* **2010**, *49*, 5706−5714. (h) Salmon, L.; Molnar, G.; Zitouni, D.; Quintero, C.; Bergaud, C.; Micheau, J. C.; Bousseksou, A. *J. Mater. Chem.* **2010**, *20*, 5499−5503. (i) Thibault, C.; Molnar, G.; Salmon, L.; Bousseksou, A.; Vieu, C. *Langmuir* **2010**, *26*, 1557−1560. (j) Tokarev, A.; Salmon, L.; Guari, Y.; Nicolazzi, W.; Molnar, G.; Bousseksou, A. *Chem. Commun.* **2010**, *46*, 8011−8013. (k) Bousseksou, A.; Molnar, G.; Salmon, L.; Nicolazzi, W. *Chem. Soc. Rev.* **2011**, *40*, 3313−3335. (l) Faulmann, C.; Chahine, J.; Malfant, I.; de Caro, D.; Cormary, B.; Valade, L. *Dalton Trans.* **2011**, *40*, 2480−2485. (m) Raza, Y.; Volatron, F.; Moldovan, S.; Ersen, O.; Huc, V.; Martini, C.; Brisset, F.; Gloter, A.; Stephan, O.; Bousseksou, A.; Catala, L.; Mallah, T. *Chem. Commun.* **2011**, *47*, 11501−11503. (n) Titos-Padilla, S.; Herrera, J. M.; Chen, X. W.; Delgado, J. J.; Colacio, E. *Angew. Chem., Int. Ed.* **2011**, *50*, 3290−3293. (o) Gural'skiy, I. A.; Quintero, C. M.; Molnar, G.; Fritsky, I. O.; Salmon, L.; Bousseksou, A. *Chem.—Eur. J.* **2012**, *18*, 9946−9954.

(10) Gadet, V.; Mallah, T.; Castro, I.; Verdaguer, M.; Veillet, P. *J. Am. Chem. Soc.* **1992**, *114*, 9213−9214.

(11) Pajerowski, D. M.; Andrus, M. J.; Gardner, J. E.; Knowles, E. S.; Meisel, M. W.; Talham, D. R. *J. Am. Chem. Soc.* **2010**, *132*, 4058−4059.

(12) Pajerowski, D. M.; Gardner, J. E.; Frye, F. A.; Andrus, M. J.; Dumont, M. F.; Knowles, E. S.; Meisel, M. W.; Talham, D. R. *Chem. Mater.* **2011**, *23*, 3045−3053.

(13) Prado, Y.; Lisnard, L.; Heurtaux, D.; Rogez, G.; Gloter, A.; Stephan, O.; Dia, N.; Rivière, E.; Catala, L.; Mallah, T. *Chem. Commun.* **2011**, *47*, 1051−1053.

(14) Prado, Y.; Dia, N.; Lisnard, L.; Rogez, G.; Brisset, F.; Catala, L.; Mallah, T. *Chem. Commun.* **2012**, *48*, 11455−11457.

(15) Dumont, M. F.; Knowles, E. S.; Guiet, A.; Pajerowski, D. M.; Gomez, A.; Kycia, S. W.; Meisel, M. W.; Talham, D. R. *Inorg Chem* **2011**, *50*, 4295−4300.

(16) The compound is made of a ferrimagnetic network, that is to say, inside the core, CoII and FeIII are in antiferromagnetic interaction (as documented in ref 2b). The shell of such a compound may by itself have a T_c if it is multidomain. If the shell is thin (here 5 nm), it is likely to behave as a single domain with a blocking temperature, when isolated from any dipolar interaction; Now, if these particles are not isolated (which is the case in the powders), the magnetic properties are commonly described as a spin glass-like behavior, that induce a "critical temperature" which is indeed close to the reported T_c. To discriminate between a T_c or a spin-glass like order provoked by the

dipolar interactions between the grains, AC susceptibility measurements should be performed (1) after irradiation (2) on highly diluted particles. This is a difficult task that is out of the range of this work. We have observed in our recent studies on much smaller CsNiCr particles that it is problematic to avoid any interactions, and in these large particles it is even more difficult. In any case, the result is a high local field up to a critical temperature that we called "ordering temperature" being not too definitive about the nature of this ordering.

(17) Presle, M.; Lemainque, J.; Guigner, J. M.; Larquet, E.; Maurin, I.; Boilot, J. P.; Gacoin, T. *New J. Chem.* **2011**, *35*, 1296−1301.

(18) Even if FT-IR does not evidence the vibrations of ferricyanide moieties, one cannot completely exclude that a small amount of remaining pairs are present, especially at the interface between the (Cs)CoFe and CsNiCr shells.

(19) Tricard, S.; Costa-Coquelard, C.; Mazerat, S.; Rivière, E.; Huc, V.; David, C.; Miserque, F.; Jegou, P.; Palacin, S.; Mallah, T. *Dalton Trans.* **2012**, *41*, 4445−4450.

(20) Our previous work on CsNiCr particles shows that there is a less than 5% deviation in composition when preparing objects ranging from 6 to 30 nm (ref 13) with $\{Cs_{0.5}NiCr_{0.95}\}$ as the average composition. This has been checked on numerous occasions by full elemental analysis and EDS measurements. The good correlation between EDS and elemental analysis led us, because of the complexity of the present heterostructures, to base our calculations on the metallic ratios determined by EDS. As all the NPs are grown from the same batch of core particles **1**, the CsNiCr cores in **2**, **3**, **2Cs**, and **3Cs** will have the same composition. The Ni/Co ratio is a molar one. The ratio calculation is based on the NP targeted size (see refs 7g and 13 for details) and represents the amounts used in the synthesis to reach the desired sizes.

(21) Using the equation described in ref 7g or 13, it is possible to correlate the size of a particle, or of a shell, with the amount of ions used in the synthesis. In the present case, the $[Fe(CN)_6]^{3-}$ complexes that remain in solution after the growth of the (Cs)CoFe layer in **2** (or in **2Cs**) lead to the formation of an interfacial NiFe layer when nickel ions are added for the growth of the external CsNiCr shell of **3** (or of **3Cs**). Knowing the amount of $[Fe(CN)_6]^{3-}$ present in solution, that is, the amount of vacancies in the (Cs)CoFe shell, the thickness of the interfacial layer can be estimated using the above-mentioned equation. In **2Cs**, 20% vacancies corresponds to 0.074 mmol of $[Fe(CN)_6]^{3-}$ in solution that will lead to a calculated 0.8 nm (so 1 nm to be realistic) NiFe layer in **3Cs**, i.e., two molecular layers. In **2**, 30% vacancies corresponds to 0.111 mmol of $[Fe(CN)_6]^{3-}$ in solution that will lead to a calculated 1.4 nm NiFe layer in **3** (so below 1.5 nm to be realistic), i.e., less than three molecular layers.

(22) As a consequence of the broadening, the size extracted when applying Scherrer's equation does not reflect the actual crystallite size. Still, an indication may be obtained on the CoFe shell by considering that the broadening is related to the larger dimension of the shell, provided that the dimension of the core is small. This gives a correlation length of 28 nm for **2** and 21 nm for **2Cs**, showing that the crystallinity is fairly good. This remains however a rough estimation.

(23) The STEM-EELS profiles are rather accidental for compound **3Cs**. This is due to the orientation of the particles that are not well aligned with the beam. Because of the weak intensity of the signal, the Ni profile is not well defined; however, the Fe and Co profiles clearly match and indicate their location in the first shell while they are absent from the external shell (since the beam probes through the whole nanoparticle, these signals are also found in the central part). The profile clearly shows that Cr is located in the outside part (the NP core represents only a very small amount of matter). It must not appear nil in any parts of the NP since the outside shell is systematically probed by the beam. However, the Cr profile is much weaker in the intermediate FeCo shell of compound **3** where the NP is well aligned with the beam.

(24) "Orientation effects" refer to what happens to a powder when not conveniently blocked. The grains inside the powder tend to orient under an applied field, and when this field is ramped down to zero, a sudden jump in the curve is observed because they recover their initial state. If the powder is immobilized with tape or in eicosane, such an event is prevented.

(25) (a) Kneller, E. F.; Hawig, R. *IEEE Trans. Magn.* **1991**, *27*, 3588−3600. (b) Zeng, H.; Li, J.; Wang, Z. L.; Liu, J. P.; Sun, S. H. *Nano Lett.* **2004**, *4*, 187−190. (c) Song, Q.; Zhang, Z. J. *J. Am. Chem. Soc.* **2012**, *134*, 10182.

(26) Volatron, F.; Heurtaux, D.; Catala, L.; Mathonière, C.; Gloter, A.; Stephan, O.; Repetto, D.; Clemente-Leon, M.; Coronado, E.; Mallah, T. *Chem. Commun.* **2011**, *47*, 1985−1987.